Cement and Concrete Research 41 (2011) 123–128

Contents lists available at ScienceDirect

Cement and Concrete Research

journal homepage: http://ees.elsevier.com/CEMCON/default.asp

A new approach in quantitative in-situ XRD of cement pastes: Correlation of heat flow curves with early hydration reactions

Christoph Hesse [1], Friedlinde Goetz-Neunhoeffer, Jürgen Neubauer *

Mineralogy, GeoZentrum Nordbayern, University of Erlangen-Nuremberg, D-91054 Erlangen, Germany

ARTICLE INFO

Article history:
Received 24 June 2010
Accepted 29 September 2010

Keywords:
Calorimetry A
Hydration A
Kinetics A
X-Ray Diffraction B
Thermodynamic Calculations B

ABSTRACT

XRD measurements of the hydration of synthetical cement (SyCem) were used to calculate the resulting heat flow from changes in the phase content. Calculations were performed by application of thermodynamic data. The comparison with data recorded from heat flow calorimetry was in good agreement with the calculated heat flow.

The initial maximum of heat flow mainly is caused by the aluminate reaction. During the entire main period the silicate reaction dominates hydration with a high and long first maximum of heat flow. The second but less intense heat flow maximum – only visible as a shoulder in most of the technical cements – can be attributed to an acceleration of the aluminate reaction with the enhanced dissolution of C_3A and the final formation of ettringite. Moreover, the investigation showed that the dissolution process of C_3A is directly controlled by the availability of the calcium sulfate phases.

© 2010 Elsevier Ltd. All rights reserved.

1. Introduction

Hydration of ordinary Portland cement (OPC) is a rather complex process which normally results in the hardening of a cement paste. During hydration the cement reacts with water resulting in the formation of the different hydrates. Ettringite ($C_3A{\cdot}3Cs{\cdot}H_{32}$) is formed from calcium sulfate, mainly tricalcium aluminate (C_3A), and water during the aluminate reaction [1]. The major calcium sulfate phases are gypsum ($Cs{\cdot}2H$), bassanite ($Cs{\cdot}0.5H$), and anhydrite (Cs) depending on the raw material and milling process of the cement. The silicate reaction describes the formation of portlandite (CH) and a C-S-H gel from the hydration of tricalcium silicate (C_3S). The composition of the C-S-H gel formed, in particular the Ca/Si ratio, is known to depend on the water to cement ratio (w/c-ratio), the temperature, and also the composition of the cement [2–4]. According to Allen et al. [5], the Ca/Si ratio is 1.7 after 28 d for a C-S-H gel from hydrated OPC at 20 °C and with w/c = 0.4.

The progress of hydration of OPC can be observed by heat flow calorimetry and X-ray diffraction (XRD) analysis. While heat flow calorimetry gives an insight into the development of the heat evolution of hydration, XRD analysis offers the possibility of time resolved determination of the phase composition in the hardening paste. By Rietveld refinement of in-situ XRD data the phase composition of the cement paste can be determined quantitatively without influencing the sample by further preparation [6]. But up to now a detailed interpretation of heat flow curves regarding the ongoing hydration reactions was not published. Thus the intension of this study was to bridge this gap by calculation of the heat flow curves from the time-dependent phase composition of the cement paste.

2. Materials and methods

2.1. Materials

Synthetic cement (SyCem) with a mineralogical composition given in Table 1 was used for the following experiments. The SyCem was produced from a synthetic clinker composed of 95 wt.-% alite and 5 wt.-% C_3A co-sintered at 1400 °C for totally 9 h in a laboratory furnace. The ground clinker was mixed with a sulfate carrier composed of 52.3 wt.-% α-bassanite and 47.7 wt.-% anhydrite II, with a total SO_3 content of 3.1 ma.-% with respect to the cement. Sulfates were synthesized at defined temperatures and characterized as described in [7]. The determined specific surface of the cement was 3700 cm^2/g (Blaine). At early times (first 22 h) the synthetic cement exhibits a hydration behavior, which is comparable to the technical white cement [8].

2.2. In-situ XRD and Rietveld analysis

Cement and water were weighted out to result in a water to cement (w/c) ratio of 0.5. For the in-situ XRD analysis a custom-made sample holder was used which controls the temperature during the measurement [8]. Two measurement temperatures were used: 23 ± 0.1 °C and

* Corresponding author. Tel.: +49 9131 85 23 986; fax: +49 9131 85 23 734.
E-mail address: neubauer@geol.uni-erlangen.de (J. Neubauer).
[1] Present address: BASF Construction Chemicals GmbH, D-83308 Trostberg, Germany.

0008-8846/$ – see front matter © 2010 Elsevier Ltd. All rights reserved.
doi:10.1016/j.cemconres.2010.09.014

Table 1
Phase composition of the SyCem. Values are given in ma.-%.

C_3S	Cubic C_3A	Anhydrite II	Bassanite
90.3	4.8	2.6	2.8

37 ± 0.3 °C. Cement and water were mixed by external stirring for 1 min before placement of the paste into the sample holder. The surface of the paste was smoothed and then covered by a 7.5 μm thick Kapton® polyimide film. The diffraction patterns were recorded by a D5000 diffractometer (Siemens) equipped with a SolX detector (Bruker) with CuK_α radiation at 40 kV and 30 mA. The measurements were carried out in a 2θ range of 7°–41° with a step width of 0.024° and 0.6 s counting time per step. 88 patterns were recorded within 22 h. The measurement of one diffraction pattern lasts approximately 15 min. Therefore the Rietveld quantification result reflects the mean of phase composition changes over a period of 15 min.

Rietveld analysis was performed with Topas 3.0 (Bruker). Details of the refinement procedure have already been described in more detail in [6]. The phase composition of the cement paste (thereafter referred to as Rietveld quantities) was calculated from the Rietveld results according to Hesse et al. [6]. All quantities are normalized with respect to the cement paste present at the time of measurement including water and C-S-H.

In addition, the phase contents of ettringite and alite were derived from the refined Rietveld scale factors (thereafter referred to as scale factor quantities). The phase content of alite was calculated for each measurement time t from the changes of the scale factors starting from a known initial (maximum) content of alite according to Eq. (1) [9]. The calculation of the ettringite content was done by assuming that all dissolved SO_3 is incorporated into ettringite and that this maximum content $(w_{Ettr})_{max}$ is achieved within 22 h. A solid solution of ettringites at the time of its maximum content was excluded by lattice parameter refinement. The maximum scale factor of ettringite was set equal to the maximum content determined after Eq. (2), where M is the molar weight and $(w_{SO_3})_{cement}$ is the total SO_3 content of the cement.

$$(w_a)_t = \frac{s_t}{s_{\max}} \cdot (w_a)_{\max} \tag{1}$$

$$(w_{Ettr})_{\max} = \frac{M(Ettringite)}{3 \cdot M(SO_3)} \cdot \left(\frac{\left(w_{so_3}\right)_{cement}}{100 + \left(\frac{w}{c} - ratio \cdot 100\right)} \right) \cdot 100\, ma.-\% \tag{2}$$

2.3. Heat flow calculation

According to Hess's law the enthalpy of reaction ΔH_R is the difference between the total of the formation enthalpies ΔH_F of the products and the starting material. The enthalpies of formation used are summarized in Table 2. The simplified main reactions during early hydration are the silicate and aluminate reactions which are described by the following equations:

silicate reaction: $C_3S + 3.9H \rightarrow C_{1.7}SH_{2.6} + 1.3CH \quad \Delta H_R = -558\ J/g$

aluminate reaction: $C_3A + 3Cs + 32H \rightarrow C_3A \cdot 3Cs \cdot H_{32} \quad \Delta H_R = -747\ J/g$

Potential time differences in dissolution–precipitation reactions were not taken into account. The value of the enthalpy of reaction is related to the solid starting material.

The heat flow for the early hydration was calculated stepwise from the changes in the quantitative phase content of alite and ettringite, which were determined by the refined Rietveld scale factors as described above. At first the quantitative data for the phase development over hydration time were smoothed by a Fourier filter. Next, the smoothed curves were differentiated with respect to time because changes in the phase content are assumed to be proportional to the heat flow curve. For calculation of the individual heat flow for the aluminate reaction based on the formation of ettringite a "heat factor" F had to be used, which describes the mass ratio between the sum of solid starting materials and the hydration product of the individual aluminate reaction (Table 3). In the case of the silicate reaction the change of the alite content could be used for the calculation directly. The individual heat flow for the reactions was calculated according to Eq. (3) where HF is the heat flow, $F_{reaction}$ is the heat factor, and ΔH_R is the enthalpy of reaction for the corresponding reaction.

$$HF = \frac{\partial(ma.-\%phase)}{\partial t} \cdot \frac{F_{reaction} \cdot \Delta H_R}{100\%} \tag{3}$$

In the last step of the heat flow calculation the individual heat flow of both the silicate and aluminate reactions is added together for a value of the total heat flow of the overall reaction. The calculated overall heat flow then can be compared with the measured heat flow recorded by a TamAir calorimeter at a temperature of 23 ± 0.1 °C and 37 ± 0.3 °C respectively.

3. Results

The Rietveld refinement of the cement paste and the following normalization of these data to a "true" phase composition of the cement paste [8] result in a curve of the changes in the composition of the cement paste over time, which shows a remarkable consistence.

At 23 °C formation of ettringite starts directly during the mixing of the cement with water (Fig. 1). Up to $t = 3$ h the ettringite content is increasing rapidly after which point the formation rate of ettringite starts decreasing. Furthermore, a constant increase in the ettringite content can be observed up to $t = 11$ h of hydration. During hydration time $t = 11$ h and $t = 14$ h the formation of ettringite is accelerated until a maximum content is reached after $t = 14$ h. After the final formation of ettringite the content is not changing up to $t = 22$ h. The progress of the aluminate reaction is accelerated with increasing temperature. For a hydration temperature of 37 °C the maximum ettringite content can be detected already after $t = 8$ h (Fig. 1) but the amount of ettringite precipitated up to $t = 1$ h is lower than at 23 °C.

Table 2
Enthalpy of formation for reactants of hydration reactions.

Phase	ΔHF [kJ/mol]	Reference
C_3S	−2929	[10]
C_3A	−3589	[11]
Cs	−1434	[12]
H	−286	[13]
CH	−986	[14]
$C_{1.7}SH_{2.6}$	−2890	[15]
Ettringite	−17,550	[16,17]

Table 3
Heat factor used for the calculation of the heat flow.

Reaction	Weight ratio	Heat factor F	
		Label	Value
Aluminate	1 g solid starting material → 1.8488 g Ettringit	$F_{aluminate}$	0.5409

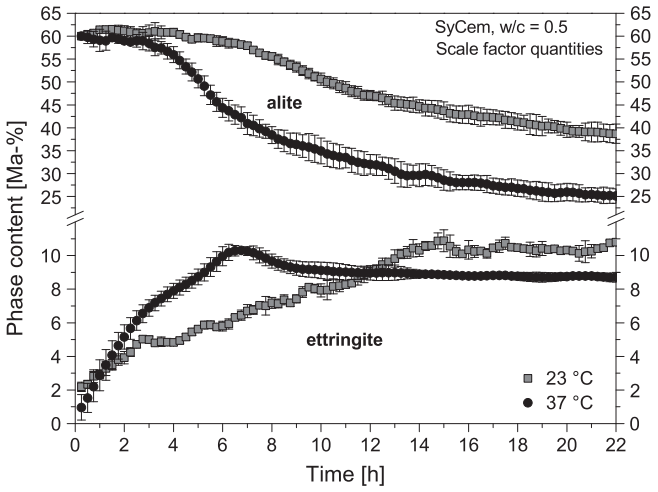

Fig. 1. Changes in the phase content of ettringite and alite at 23 °C and 37 °C for the hydration of the SyCem derived from the scale factors. The curves result from the average of three measurements and the error bars represent the respective standard deviations.

After that hydration phase the ettringite content shows a decrease and monosulfate is starting to form together with ettringite.

Also the silicate reaction is strongly affected by the temperature. At a temperature of 23 °C the alite content shows no changes from the beginning of hydration up to $t = 4$ h (Fig. 1). After this time the onset of dissolution of alite is detectable. The alite dissolution is then accelerated up to $t = 9$ h of hydration and finally the dissolution slows down. Within the first 22 h of hydration approximately 40% of the initial alite content of 60 ma.-% is calculated to be dissolved. At 37 °C the dissolution of alite starts at around $t = 2$ h and the dissolution rate is increased (Fig. 1). Within 22 h of hydration 55% of crystalline, and thus detectable, alite is dissolved.

The aluminate reaction can also be observed by changes in C_3A and the anhydrite content (Fig. 2). At 23 °C and 37 °C bassanite is completely dissolved within the first minutes of hydration and hence that phase was not detectable by XRD anymore. The second sulfate phase – anhydrite – is not dissolved up to $t = 2$ h at 23 °C. With proceeding hydration anhydrite dissolves rapidly and is not detected after $t = 12$ h. The dissolution of C_3A is very fast and starts directly after contact with water. During the first hour of hydration the C_3A content decreases by about 1 ma.-% from the initial content of ca. 3.2 ma.-% in the cement paste. Between $t = 1$ h and $t = 12$ h the C_3A content remains at ca. 2 ma.-%. After complete dissolution of anhydrite a strong decrease in the C_3A content is observed between $t = 12$ h and $t = 14$ h. Furthermore, after $t = 14$ h the dissolution rate slows down and C_3A is completely dissolved after 20 h.

The same sequence of processes can also be observed at a temperature of 37 °C. At increased temperatures the initial dissolution of C_3A after contact with water runs faster and therefore a smaller amount of C_3A is observed in the first measurement after $t = 0.25$ h. An important observation is that, according to Fig. 2, as long as anhydrite is available in the paste C_3A does not appear to dissolve. This behavior has also been observed by Minard et al. [18] Moreover, the dissolution of C_3A proceeds faster with increasing temperature.

From the curves of alite and ettringite content the heat flow curves were calculated for 23 °C and 37 °C, respectively. Fig. 3 for example represents the single heat flow curves for the aluminate reaction calculated from the formation of ettringite and the single heat flow for the silicate reaction derived from the decrease observed in alite content at 23 °C. It is an important finding that the total calculated heat flow and the measured heat flow are in fair agreement. The initial heat flow mainly is a result of the aluminate reaction — resulting in the formation of ettringite. In addition the aluminate reaction shows a strong effect at the end of the main hydration period at $t = 12$ h. The second heat flow maximum is apparently caused by an acceleration of the aluminate reaction with an enhanced C_3A dissolution. The end of the aluminate reaction with the final formation of ettringite is completed after $t = 15$ h. On the other hand the silicate reaction dominates the whole main period. As shown in detail in Fig. 3 the silicate reaction starts to produce more heat flow at $t = 3$ h, which correlates with the end of the induction period. This accelerated period of the reaction continues until $t = 9$ h. After that time the dissolution rate of alite decreases and hence the heat flow from the silicate reaction decreases. The remaining heat flow is still due to the silicate reaction and the low value of 1 mW/g suggests that at this time the reaction proceeds diffusion controlled.

The calculated heat flow at an elevated temperature of 37 °C also is in fair correlation with the measured heat flow from calorimetry (Fig. 4). In the same way as was observed at 23 °C the main period is dominated by a very fast silicate reaction resulting in a narrow but high heat flow maximum. The progress of the aluminate reaction is similar to the reaction at 23 °C. After the completed dissolution of sulfate the final formation of ettringite is connected with an increase

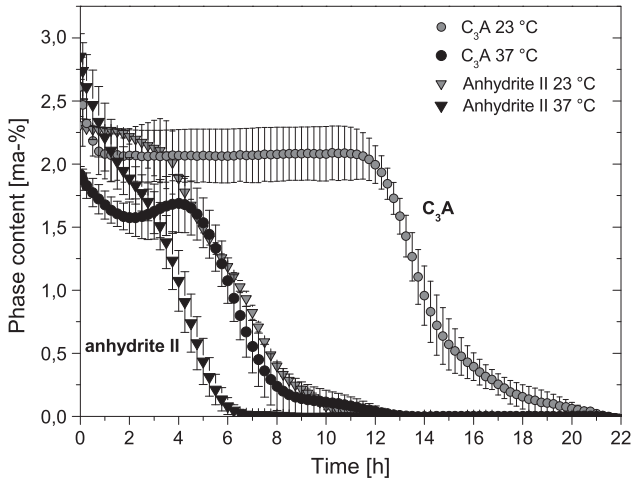

Fig. 2. Changes in Rietveld quantities of anhydrite II and cubic C_3A during the early hydration of the SyCem at 23 °C and 37 °C. The curves result from the average of three measurements and the error bars represent the respective standard deviations.

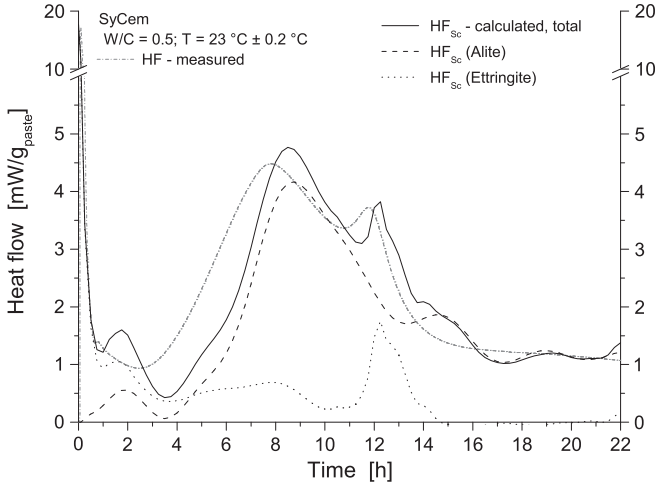

Fig. 3. Comparison between measured and calculated heat flow curves at 23 °C. In addition, the heat flow for the silicate (alite) and the aluminate (ettringite) reaction is shown. HF_{Sc}…heat flow was calculated from the scale factor quantities.

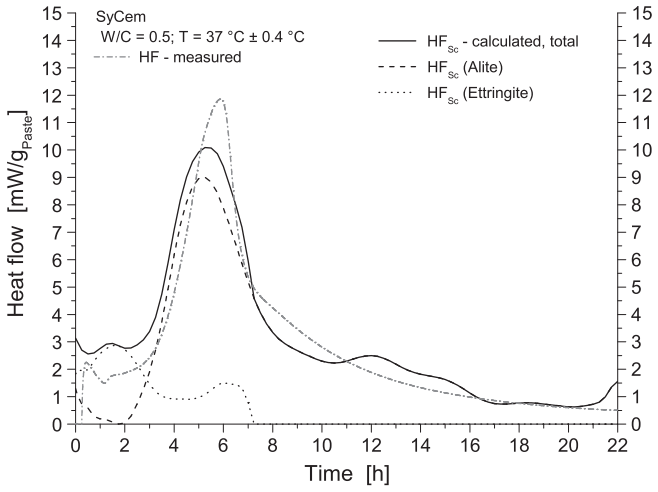

Fig. 4. Comparison between measured and calculated heat flow curves at 37 °C. In addition, the heat flow for the silicate (alite) and the aluminate (ettringite) reaction is shown. HF_{Sc}…heat flow was calculated from the scale factor quantities.

in heat flow at the end of the main period. Between $t=7$ h and $t=12$ h the calculated heat flow is lower than expected from calculations.

4. Discussion

The calculated heat flow allows a fair visualization of the two different hydration reactions during early hydration. The induction period is dominated by dissolution of bassanite and C_3A and the rapid formation of ettringite. According to our results the initial heat flow of 20 mW/g$_{paste}$ is mainly related to dissolution of C_3A. The total heat of hydration at 23 °C between $t=0$ h and $t=0.5$ h is 10.8 J/g. This is lower than the calculated heat of dissolution of C_3A, anhydrite, and bassanite (Table 4) at 23 °C. This difference is caused by external preparation and measurement of heat flow artifacts. The dissolution of cement phases starts directly after addition of water to the cement powder and the first formation of new precipitates like ettringite starts. During stirring of the paste some heat is released which cannot accurately be measured.

After the initial period heat flow decreases to lower values and the induction period starts. The formerly used phrase “dormant period” is not sufficient to describe the processes taking place during the induction period. Actually this period is a result of the slowdown in the C_3A hydration. Different models exist for this slowdown in the literature [21,22]. Due to an increase in the sulfate concentration in the pore solution the dissolution of C_3A nearly comes to a halt and the formation rate of ettringite decreases which results in a lower but constant rate until final formation of ettringite is complete. As shown in Fig. 1, the amount of ettringite increases during that time whereas no C_3A is dissolved (Fig. 2). In addition, if all dissolved C_3A was to be converted into ettringite the amount of ettringite formed during the initial period would have to be higher, than actually observed.

Table 4
Changes in phase content of dissolving phases between $t=0$ h and $t=0.5$ h during early hydration at 23 °C and the derived calculated heat of the solution (thermodynamic data for heat of the solution from [19] for C_3A and [20] for sulfates).

Phase	Initial content [ma.-%]	Content after 0.5 h [ma.-%]	Consumption [ma.-%]	Released heat by dissolution [J/g$_{paste}$]
C_3A	3.1	2.1	1.0	−30.6
Anhydrite	3.2	2.2	1.0	−1.6
Bassanite	1.8	0.0	0.7	−1.8
Total				−32.9

Therefore, we assume the formation of an amorphous aluminate phase which can serve as a reservoir for further ettringite formation after the initial period. Due to the reduced maximum concentration of aluminum ions in the pore solution observed by [23,24] the presence of this intermediate phase is possible. The existence of hydrated aluminate phases was also observed by Black et al. [25] during their investigation of the hydration of C_3A both in the absence and presence of calcium sulfate. The authors found the formation of a small amount of C_4AH_{19} beside the formation of ettringite. In our study no XRD reflections of C_4AH_{19} were recorded and no crystalline aluminate hydrate was identified.

The constant formation rate of ettringite between $t=2$ and $t=12$ h at 23 °C appears to be the result of the ongoing consumption of the amorphous aluminate reservoir and anhydrite. After $t=12$ h and the complete dissolution of anhydrite the dissolution of C_3A is restarted again and a large amount of ettringite is precipitated from previously dissolved SO_4^{2-} and Ca^{2+}. After the final formation of ettringite which is accompanied by a strong increase in heat flow due to the dissolution of C_3A, the concentration of the SO_4^{2-} concentration in the pore solution of the cement paste decreases. At this stage little C_3A is still present in the cement paste and a conversion of ettringite to monosulfate should start. This reaction can be proven by the occurrence of monosulfate reflections in the diffraction patterns (Fig. 5) but is observed only at 37 °C. In contrast, at 23 °C the conversion is not detectable and the ettringite remains stable up to 22 h. The determination of the monosulfate content by Rietveld refinement is limited due to the absence of a valid structure model for monosulfate-14H, which was detected in the pastes.

Synchronous as the aluminate reaction, the silicate reaction proceeds with the formation of CH and C-S-H. The silicate reaction can be divided into three separate periods: (i) induction period between $t=0$ and $t=2$ h (23 °C), (ii) acceleration period between

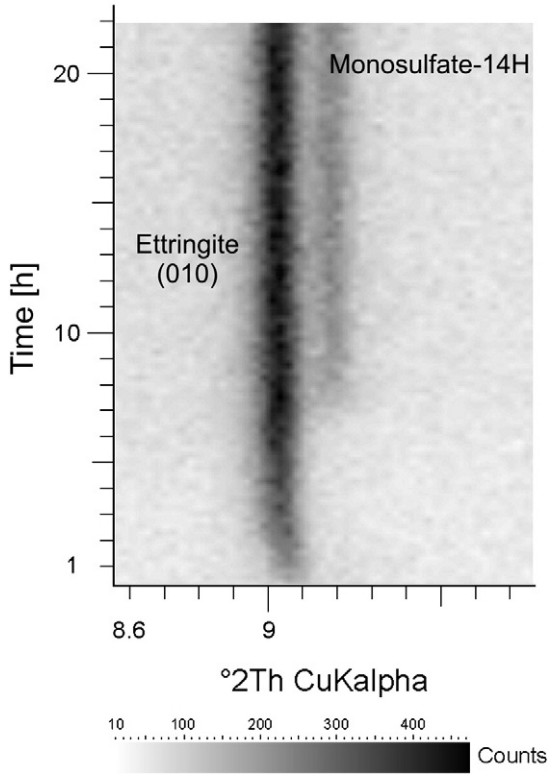

Fig. 5. Time-dependent changes in the in-situ XRD pattern of ettringite (010) and monosulfate (006) reflections at 37 °C. The formation of monosulfate occurs after the final formation of ettringite.

$t=2$ and $t=8$ h (23 °C) and (iii) slow down phase after $t=8$ h (23 °C). The silicate reaction starts directly after contact with water which can be observed during the hydration of pure C_3S. We assume that in the first stage of hydration the silicate reaction is initialized by the start of the dissolution process of C_3S and the formation of the first nuclei of C-S-H without the appearance of CH according to Damidot and Nonat [26]. The dissolution of alite can only be observed at 37 °C, where a small decrease in the alite content is calculated from the refinement of the X-ray data. But Julliand et al. [27] observed the dissolution of alite also at 20 °C in the first minutes of hydration with an increase in the calcium concentration in the pore water. They conclude that the initial and dormant period is mainly controlled by the dissolution processes of alite. The duration of the dormant period depends directly on the availability of reactive nuclei as shown by Thomas et al. [28]. With the addition of synthetic C-S-H seeds they have shown a shortening of the dormant period and also an influence on the acceleration phase. From the results of Thomas et al. [28] and Alizadeh et al. [29] together with our observations, we assume that the end of the dormant period and the start of the acceleration phase after $t=2$ h (at 23 °C) are directly connected to the formation of stable C-S-H seeds, which have exceeded a critical number enough for the acceleration of the hydration. A second activator for the start of the acceleration phase is the slowdown in the aluminate reaction, supporting a higher availability of Ca^{2+} ions in the pore solution for the silicate reaction. The acceleration phase of the silicate reaction is directly connected to a strong decrease in the content of alite and hence an increase in CH and C-S-H content.

With further progress of the acceleration phase the amount of free water in the cement paste is reduced and the rate of the dissolution–precipitation process is slowing down until hydration becomes diffusion controlled. This kind of reaction is reached after $t=8$ h at 23 °C where around 20% of the initial water is used up by the formation of the hydrate phases. As a consequence of the reduction of pore volume during the formation of the hydrate phases, the formation rate of the hydrates might be retarded.

The processes of both the aluminate and silicate reactions are depending directly on the temperature. At a higher temperature all processes run faster as described in previous published results [8,24,30,31]. The influence of the temperature on both reactions (aluminate and silicate reactions) is comparable but, depending on the sulfate carrier composition, the dissolution of the sulfate phase can show different effects at different temperatures.

The progress of the hydration reactions and their contribution to the total heat flow are shown schematically in Fig. 6.

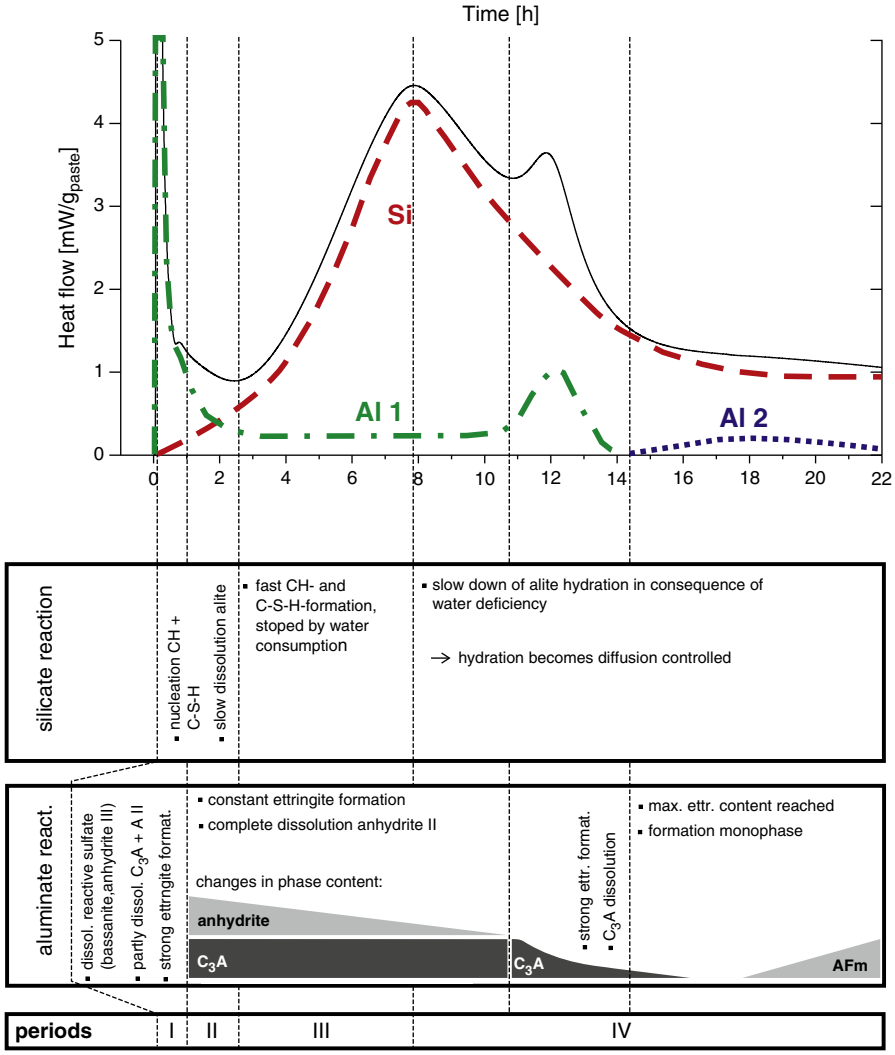

Fig. 6. Interpretation of the total heat flow during early hydration of OPC from the result of this work for hydration at 23 °C. The contribution of the silicate reaction (Si) and aluminate reactions (Al1, Al2) to the total heat flow is indicated by dotted and dashed lines, respectively. I — initial period, II — induction period, III — acceleration phase, and IV — slow down phase (nomenclature according to Taylor [1]).

5. Conclusion

The new method of combining XRD and calorimetric data shown above gives a good insight into processes taking place during early OPC hydration (first 22 h). The described heat flow calculation method from phase composition changes enables the possibility of fast interpretation of heat flow events even in complicated systems such as OPC-based tile adhesives or concrete. Based on few assumptions, the results of the quantitative in-situ XRD analysis do lead to a better understanding of these processes. The resulting model proposed shows a more complex course of the aluminate and silicate reactions than previously published. The second heat flow event at the end of the main period of hydration is definitely based on the final ettringite formation due to a renewed dissolution of C_3A. We showed that the dissolution process of C_3A is directly controlled by the availability of the soluble calcium sulfate phases such as bassanite and anhydrite.

The present results enable a much better interpretation of calorimetric data, which is related directly to the possibility of determining the phase composition in a cement paste with in-situ laboratory XRD measurements. The method will be further improved in the future in order to achieve a higher accuracy of the refined values of quantitative phase contents. For that purpose the method will also be adapted on more realistic systems including commercial OPC and ternary binder systems containing high alumina cement, sulfates and OPC.

Acknowledgments

We thank BASF Construction Chemicals GmbH for funding this work. Further we thank Dr. Michael Melchart for helpful comments on the script.

References

[1] H.F.W. Taylor, Cement Chemistry, 2nd ed, Thomas Telford Publishing, 1997.
[2] J.I. Escalante-Garcia, J.H. Sharp, Variation in the composition of C-S-H gel in Portland cement pastes cured at various temperatures, J. Am. Ceram. Soc. 82 (1999) 3237–3241.
[3] I.G. Richardson, The nature of C-S-H in hardened cements, Cem. Concr. Res. 29 (1999) 1131–1147.
[4] I.G. Richardson, The calcium silicate hydrates, Cem. Concr. Res. 38 (2008) 137–158.
[5] A.J. Allen, J.J. Thomas, H.M. Jennings, Composition and density of nanoscale calcium–silicate–hydrate in cement, Nat. Mater. 6 (2007) 311–316.
[6] C. Hesse, F. Goetz-Neunheoffer, J. Neubauer, M. Braeu, P. Gaeberlein, Quantitative in-situ X-ray diffraction analysis of early hydration of Portland cement at defined temperatures, Powder Diffr. 24 (2009) 112–115.
[7] S. Seufert, C. Hesse, F. Goetz-Neuhoeffer, J. Neubauer, Quantitative determination of anhydrite III from dehydrated gypsum by XRD, Cem. Concr. Res. 39 (2009) 936–941.
[8] C. Hesse, M. Degenkolb, P. Gäberlein, F. Götz-Neunheoffer, J. Neubauer, V. Schwarz, Investigation into the influence of temperature and w/c ratio on the early hydration of white cement, Cement Int.l 6 (2008) 68–78.
[9] M. Merlini, G. Artioli, T. Cerulli, A. Bravo, F. Cella, Tricalcium aluminate hydration in additivated systems. A crystallographic study by SR-XRPD, Cem. Concr. Res. 38 (2008) 477–486.
[10] D.D. Wagman, W.H. Evans, V.B. Parker, R.H. Schumm, I. Halow, S. Bailey, K. Churney, R. Nuttall, The NBS tables of chemical thermodynamic properties. Selected values for inorganic and C1 and C2 organic substances in SI units, J. Phys. Chem. Ref. Data Supplement 11 (S2) (1982) 1–392.
[11] W. Zhuang, J. Liang, Z. Qiao, J. Shen, Y. Shi, G. Rao, Estimation of the standard enthalpy of formation of double oxide, J. Alloys Compd. 167 (1998) 6–10.
[12] J. Majzlan, A. Navrotsky, J.M. Neil, Energetics of anhydrite, barite, celestine, and anglesite: a high-temperature and differential scanning calorimetry study, Geochim. Cosmochim. Acta 66 (2002) 1839–1850.
[13] A.F. Holleman, E. Wiberg, N. Wiberg, Lehrbuch der anorganischen Chemie, Vol. 100, Walter de Gruyter, 1985.
[14] R.A. Robie, B.S. Hemingway, J.R. Fisher, Thermodynamic properties of minerals and related substances at 298.15 K and 1 Bar (105 Pascals) pressure and at higher temperatures, US Geological Survey Bulletin-Report 1452, 1978.
[15] K. Fujii, W. Kondo, Communications of the American Ceramic Society: Estimation of thermochemical data for calcium silicate hydrate (C-S-H), J. Am. Ceram. Soc. 66 (1983) C–220-C-221.
[16] H.A. Berman, E.S. Newman, Heat of formation of calcium aluminate monosulfate at 25 °C, J. Res. Nat. Bur. Stand. 67A (1963) 1–13.
[17] R.B. Perkins, C.D. Palmer, Solubility of ettringite ($Ca_6Al_2(SO_4)_3(OH)_{12}$ $26H_2O$) at 5–75 °C, Geochim. Cosmochim. Acta 63 (1999) 1969–1980.
[18] H. Minard, S. Garrault, L. Regnaud, A. Nonat, Mechanisms and parameters controlling the tricalcium aluminate reactivity in the presence of gypsum, Cem. Concr. Res. 37 (2007) 1418–1426.
[19] T. Thorvaldson, W.G. Brown, C.R. Peaker, Studies on the thermochemistry of the compounds occurring in the system $CaO–Al_2O_3–SiO_2$. IV. The heat of solution of tricalcium aluminate and its hydrates in hydrochloric acid, J. Am. Chem. Soc. 52 (1930) 3927–3936.
[20] R.H. Perry, D.W. Green, Perry's Chemical Engineers Handbook, 7th edition, 1997.
[21] Rilem Technical Committee, The hydration of tricalcium aluminate and tetracalcium aluminoferrite inthe presence of calcium sulfate, Mater. Struct. 19 (1986) 137–147.
[22] P.W. Brown, Kinetics of tricalcium aluminate and tetracalcium aluminoferrite hydration in the presence of calcium sulfate, J. Am. Ceram. Soc. 76 (1993) 2971–2976.
[23] D. Rothstein, J.J. Thomas, B.J. Christensen, H. Jennings, Solubility behavior of Ca-, S-, Al-, and Si-bearing solid phases in Portland cement pore solutions as a function of hydration time, Cem. Concr. Res. 32 (2002) 1663–1671.
[24] J.J. Thomas, D. Rothstein, H.M. Jennings, B.J. Christensen, Effect of hydration temperature on the solubility behavior of Ca-, S-, Al-, and Si-bearing solid phases in Portland cement pastes, Cem. Concr. Res. 33 (2003) 2037–2047.
[25] L. Black, C. Breen, J. Yarwood, C.S. Deng, J. Phipps, G. Maitland, Hydration of tricalcium aluminate (C_3A) in the presence and absence of gypsum — studied by Raman spectroscopy and X-ray diffraction, J. Mater. Chem. 16 (2006) 1263–1272.
[26] D. Damidot, A. Nonat, C_3S hydration in diluted and stirred suspensions, Adv. Cem. Res. 6 (1994) 27–35.
[27] P. Julliand, E. Gallucci, R. Flatt, K. Scrivener, Dissolution theory applied to the induction period in alite hydration, Cem. Concr. Res. 40 (2010) 831–844.
[28] J.J. Thomas, H.M. Jennings, J.J. Chen, Influence of nucleation seeding on the hydration mechanisms of tricalcium silicate and cement, J. Phys. Chem. C 113 (2009) 4327–4334.
[29] R. Alizadeh, L. Raki, J.M. Makar, J.J. Beaudoin, I. Moudrakovski, Hydration of tricalcium silicate in the presence of synthetic calcium–silicate–hydrate, J. Mater. Chem. 19 (2009) 7937–7946.
[30] J.I. Escalante-Garcia, J.H. Sharp, Effect of temperature on the hydration of the main clinker phases in Portland cements: Part I, neat cements, Cem. Concr. Res. 28 (1998) 1245–1257.
[31] B. Lothenbach, F. Winnefeld, C. Alder, E. Wieland, P. Lunk, Effect of temperature on the pore solution, microstructure and hydration products of Portland cement pastes, Cem. Concr. Res. 37 (2007) 483–491.